Dept. of Math./CMA
Pure Mathematics
ISSN 0806–2439

University of Oslo
No 1
January 2010

Convergence of the MPFA O-method on general grids

Runhild A. Klausen[1] and Annette F. Stephansen[2]

[1] Centre of Mathematics for Applications, University of Oslo, P.Box 1053 Blindern, N-0316 Oslo, Norway.

[2] Centre for Integrated Petroleum Research, University of Bergen, N-5007 Bergen, Norway.

Abstract

The analysis of the Multi point flux approximation (MPFA) method has so far relied on the possibility of seeing it as a mixed finite element method for which the convergence is then established. This type of analysis has been successfully applied to triangles and quadrilaterals, lately also in the case of rough meshes.

Another well known conservative method, the mimetic finite difference method, has also traditionally relied on the analogy with a mixed finite element method to establish convergence. Recently however a new type of analysis proposed by Brezzi, Lipnikov and Shashkov (2005), permits to show convergence of the mimetic method on a general polyhedral mesh.

We propose to formulate the MPFA O-method in a mimetic finite difference framework, in order to extend the proof of convergence to polyhedral meshes. The formulation is useful to see the close relationship between the two different methods and to see how the differences lead to different strenghts. We pay special attention to the assumption needed for proving convergence by examining various cases in the section dedicated to numerical tests.

1 Introduction

Control volume methods are frequently used in reservoir simulation in order to solve the elliptic pressure equation derived from Darcy's law. This family of methods conserve mass locally, which is important since the elliptic equation is coupled with a hyperbolic conservation law describing the saturation in multiphase flow. The layers and fractures in the geological domain as well as the interaction between different phases lead to anisotropies and heterogeneities in the permeability tensor K, which can be challenging for the method. Another factor to consider is the complex geometry and its coupling with wells which lead to the use of grids that can be rough also upon refinement. Finally, if

the method provides local explicit fluxes we have the possibility of solving the coupled saturation equation implicitly.

When examining control volume methods it is useful to classify them into and K^{-1}- and K-methods as is done by Klausen and Russell[18]. In the former category we find methods that calculate the pressure gradients in terms of the fluxes, that is $\nabla p = K^{-1}u$, like the mixed finite element method and the mimetic finite difference method. The K-methods calculate the fluxes in terms of the pressure gradients, that is $u = K\nabla p$, and amongst these methods we find the multi-point flux approximation (MPFA) methods and the more traditional two-point flux approximation (TPFA) method.

The MPFA methods are a generalization of the TPFA method which is often used by the oil industry to discretize the pressure equation. While the MPFA methods are more costly in terms of computations, they are designed to be exact for linear pressure fields also when the principal axes of the permeability are not aligned with the grid. This is not the case for the TPFA method, as shown by Aavastmark [4]. As the TPFA method, the MPFA methods provide local explicit fluxes with respect to the pressure. Additionally then, the MPFA methods perform well even on rough grids and on grids that are not K-orthogonal. The formulation of the MPFA method usually leads to a non-symmetric method.

The first MPFA methods were presented in 1994 by Aavatsmark, Barkve, Bøe and Mannseth [5] and by Edwards and Rogers [9]. Subsequent developements include amongst others [1], [2], [15]. Several different stencils have been proposed, most notably the generalization of the original O-method, the θ methods (see for instance [26] and [17]), and the L-method [12]. Numerical tests have examined convergence and robustness on various types of grids and with a discontinuous and/or anisotropic permeability tensor, see for instance the work by Eigestad og Klausen [10].

Considering the theoretical convergence analysis, initial attempts sought how to reconstru'ct an interior vector field compatible with the fluxes which would recast the MPFA method as a mixed finite element method. An example of how the standard MPFA O-method is recast as a MFE method on triangulations can be found in [22]. In [19, 23], examining quadrilaterals, an MPFA method which is derived from a mapping onto an orthogonal reference cell is analyzed. However, the analysis requires asymptotic h^2–parallelogram meshes, or so called smooth meshes. In a successive paper convergence is proved for the O-method on rough grids [20]. In both of these papers the analysis is confined to the 2D case. On triangulations symmetric MPFA methods are available without similar asymptotic mesh-restrictions, and convergence can be showed, cf. [17]. A limitation in the convergence study based on the analogy with mixed finite elements is thus its limitation to triangles and quadrilaterals and the difficulty of extending the proof to three dimensional space.

A new proof of convergence of the MPFA O-method on general grids has been presented recently by Agelas and Masson [14]. Here they show weak convergence of the gradient, but do not provide rate of convergence of the fluxes. Their proof is however valid on heterogeneous permeability fields and is not based on similarities with the MFE methods.

While the mixed FE method defines a continuous vector velocity field, the mimetic finite difference method uses a velocity field which is only defined on element interfaces. Another property in common with the MPFA methods is that the MFD method is designed to be exact for linear pressure fields. The mimetic finite difference method has been successfully applied to diffusion problems with strong heterogeneities, see for instance [25] and [24], but does not in general allow for the definition of an explicit flux as a function of local pressure values. The symmetry of the method makes it particularly robust when dealing with anisotropies. While earlier proves of convergence relied on a comparison with the MFE method, the paper of Brezzi, Lipnikov and Shashkov [7] provides a rigorous proof of convergence for the MFD method for general polyhedra, where the need for element interpolation is eliminated. In their following paper [8] the proof is also extended to curved interfaces.

In this paper we show that the MPFA O-method in 2D and 3D can be written as a MFD method by using the quadrature rule presented in [20]. The 2D case was earlier presented in [11]. This formulation also coincides with the Local Flux Mimetic Finite difference method as presented by Lipnikov, Shashkov and Yotov [13], with the exception that the MPFA method uses fluxes and not a discrete normal velocity field as the unknown. When the interface is plane this is just a difference in scale. We do not propose to solve the MPFA method in this manner, but rather use the reformulation to prove convergence and better understand the working of the method. The non-symmetry of the method means that the convergence proof presented by Brezzi, Lipnikov and Shashkov for the MFD method [7] must be slightly modified.

An important aspect is however on what grids and with what anisotropies the convergence proof is valid, and whether the proof is sharp. We therefore examine the convergence of the pressure and of the flux using a comparable norm on a grid where the assumption necessary for the convergence proof is no longer satisfied. Other numerical tests showing the convergence of the method have not been carried out as these can be found in other papers (see previous references and the references therein). We do not consider heterogeneous permeability fields.

The paper is organized as follows: Paragraf 2 presents the model problem and setting. Paragraf 3 provides the convergence proof, while paragraf 4 presents numerical tests which provide the basis for discussing the validity of the convergence proof.

2 Model problem and setting

2.1 Continuous problem

For simplicity of exposition we will limit our discussion to Dirichlet boundary conditions. Let Ω be a domain in $\mathbb{R}^d$, $d \in \{2, 3\}$, with polygonal boundary $\partial\Omega$. We consider the following elliptic equation with homogeneous Dirichlet

boundary conditions:

$$\begin{cases} -\nabla\cdot(K\nabla p) = f & \text{in } \Omega, \\ p = 0 & \text{on } \partial\Omega. \end{cases} \tag{1}$$

Viewing (1) as the prototype for the pressure equation in porous medium flow, we can identify p as the pressure, K as the permeability tensor and f as a source term.

The mixed formulation of (1) is obtained by introducing the unknown Darcy velocity $\mathbf{u} = -K\nabla p$ as a new variable. We seek $(\mathbf{u}, p) \in H(\mathrm{div}, \Omega) \times L^2(\Omega)$ such that

$$\begin{cases} (K^{-1}\mathbf{u}, \mathbf{v})_{0,\Omega} - (p, \nabla\cdot\mathbf{v})_{0,\Omega} = 0, & \forall \mathbf{v} \in H(\mathrm{div}, \Omega), \\ (\nabla\cdot\mathbf{u}, q)_{0,\Omega} = (f, q)_{0,\Omega} & \forall q \in L^2(\Omega), \end{cases} \tag{2}$$

supplied by boundary conditions, where $f \in L^2(\Omega)$ and K is a symmetric, positive definite field in $[W^1_\infty(\Omega)]^{2,2}$ whose smallest eigenvalue is bounded from below by a positive constant. The subscript $0, \Omega$ denotes the L^2-scalar product on Ω. Similarly, the subscript $0, R$ indicates the the L^2-scalar product and its associated norm on a subset $R \subset \Omega$. For $s \geq 1$, a norm (semi-norm) with the subscript s, R designates the usual norm (semi-norm) in $H^s(R)$.

2.2 Discrete setting and interpolation

Regarding notation, a tilde will indicate an integrated quantity, such as fluxes or a normal integrated over the corresponding (partial) face. The subscript h indicates a member of the discrete space, while bolds will indicate a vector. Let $\{\mathcal{P}_h\}_{h>0}$ be a shape-regular family of affine polyhedral meshes of the domain Ω. Let each polyhedron be such that a maximum of d faces meet in a vertex (node). This is always the case in $2D$. A generic element in $\mathcal{P}_h$ is denoted by E, h_E denotes the diameter of E and $\mathbf{n}^E$ its outward unit normal. Set $h = \max_{E\in\mathcal{P}_h} h_E$. Let k be the index of the nodes of the polyhedron E, while i is the index of the polygons which constitute the faces of the polyhedron. The nodes of the element form the set $\mathcal{N}^E$, while the nodes of the face F_i form the set $\mathcal{N}^E_i$. Let $\bar{\mathbf{x}}^E_i$ identify the barycenter of the face F_i, $\bar{\mathbf{x}}^E_e$ the midpoint of an edge e, while $\bar{\mathbf{x}}^E_0$ designates the barycenter of the polyhedral element. The barycenter of the element will also be used as the local origin. We partition the polyhedron into sub-cells E_k, one for each vertex k of the element, by using the barycenters $\bar{\mathbf{x}}^E_i$, $\bar{\mathbf{x}}^E_e$, $\bar{\mathbf{x}}^E_0$ and the vertexes k. An external face of a sub-cell will be a subset of an element face and delimited by: the vertex k, the barycenter of the face $\bar{\mathbf{x}}^E_i$ and the midpoints $\bar{\mathbf{x}}^E_{e1}$ and $\bar{\mathbf{x}}^E_{e2}$ where $e1$ and $e2$ are the edges of i that meet in vertex k. We will denote these partial faces by F_{ik}. In $3D$, F_{ik} are quadrilaterals and E_k are hexahedra. In $2D$, F_{ik} are line-segments, while E_k are quadrilaterals. For each couple of faces $i1$, $i2$ that share an edge e we construct a (bilinear) internal face by connecting $\bar{\mathbf{x}}^E_e$, $\bar{\mathbf{x}}^E_{i1}$, $\bar{\mathbf{x}}^E_{i2}$ and $\bar{\mathbf{x}}^E_0$. To each of the faces F_{ik} (subsets of F_i) we associate the normal $\tilde{\mathbf{n}}_{ik}$ which is $\mathbf{n}^E_i$ (the

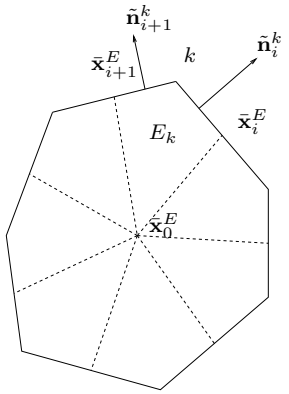

Nomenclature in $2D$

normal of F_i) integrated over the external partial face F_{ik}. An illustration for the $2D$ case is found in Figure 2.2, where $\tilde{\mathbf{n}}_{ik}$ has the dimension of a length.

We consider the space X_h of discrete pressures that are constant on each element E, that is,

$$X_h = \{q_h \in L^2(\Omega); \forall E \in \mathcal{P}_h, q_h|_E \in \mathbb{P}_0\}.$$

where $\mathbb{P}_0$ indicates polynomials of degree 0. Our velocity space V_h consists of discrete velocity vectors defined only on the partial faces F_{ik} (edges in $2D$) of the element and are aligned with the average normal of the partial face. To each face F_i of the element E we thus associate $m_i = \#\mathcal{N}_i^E$ unknowns, where $\#\mathcal{N}_i^E$ is the number of vertexes of the face i. These unknowns are the (scalar) partial fluxes $\tilde{v}_{ik}^E$, $k \in \mathcal{N}_i^E$. The discrete velocity field is thus defined by its components that are piecewise constant on a face and equal to

$$\mathbf{v}_{ik}^E = \frac{1}{|F_{ik}|} \tilde{v}_{ik}^E \hat{\mathbf{n}}_{ik}^E \tag{3}$$

where

$$\hat{\mathbf{n}}_{ik}^E = \frac{\tilde{\mathbf{n}}_{ik}^E}{|\tilde{\mathbf{n}}_{ik}^E|} = \frac{\tilde{\mathbf{n}}_{ik}^E}{|F_{ik}|}$$

is the unit average normal vector on the partial face F_{ik}. In addition, conservation of flux is imposed directly on the partial fluxes. This imposes continuity of the normal component of the velocity field. As fluxes aligned with the outward normal are defined as positive, on a partial side shared by two elements the sum of the corresponding partial fluxes must be equal to zero. We also define the flux $\tilde{v}_i$ over the face F_i equal to the sum of the corresponding partial fluxes, i.e.

$$\tilde{v}_i^E = \sum_{k \in \mathcal{N}_i^E} \tilde{v}_{ik}^E. \tag{4}$$

The superscript E will henceforward be omitted if there is no ambiguity in order to facilitate reading. The partial side fluxes are regrouped into the vector $\tilde{\mathbf{v}}$, while the restriction of $\tilde{\mathbf{v}}$ to the d partial fluxes on the faces F_{ik} that share a vertex k is indicated by $\tilde{\mathbf{v}}_k$.

To comply with the mimetic finite difference setting, we define the discrete divergence of $\mathbf{v}_h \in V_h$ as an operator $\nabla_h : V_h \mapsto X_h$ such that on each $E \in \mathcal{P}_h$

$$\nabla_h \cdot \mathbf{v}_h|_E \equiv \frac{1}{|E|} \sum_{F_i \in \partial E} \tilde{v}_i^E = \frac{1}{|E|} \sum_{F_i \in \partial E} \sum_{k \in \mathcal{N}_i^E} \tilde{v}_{ik}^E. \tag{5}$$

Finally we define the interpolation operator $\mathcal{I}$ of any vector-valued function $\mathbf{v} \in H(\mathrm{div}, \Omega)$ so that $\mathbf{v}^{\mathcal{I}} \in V_h$ and

$$(\mathbf{v}^{\mathcal{I}})_{ik} = \frac{1}{|F_{ik}|} (\mathbf{v} \cdot \mathbf{n}_i^E, 1)_{0,F_{ik}} \hat{\mathbf{n}}_{ik} \quad \forall E \in \mathcal{P}_h, \forall F_{ik} \in F_i. \tag{6}$$

The interpolation thus gives a piece-wise constant velocity vector directed in the average normal direction of the sub-face F_{ik}, given by the average flux divided by the area. An important property of this interpolation is that the flux over each sub-face F_{ik} (and thus over each face $F_i \in \partial E$) is preserved, i.e.

$$\begin{aligned} ((\mathbf{v}^{\mathcal{I}})_{ik} \cdot \mathbf{n}_i^E, 1)_{0,F_{ik}} &= (\mathbf{v}^{\mathcal{I}})_{ik} \cdot \tilde{\mathbf{n}}_{ik} = \frac{1}{|F_{ik}|} (\mathbf{v} \cdot \mathbf{n}_i^E, 1)_{0,F_{ik}} \hat{\mathbf{n}}_{ik} \cdot \tilde{\mathbf{n}}_{ik} \\ &= (\mathbf{v} \cdot \mathbf{n}_i^E, 1)_{0,F_{ik}} \end{aligned} \tag{7}$$

It immediately follows that the discrete divergence (defined in (5)) of the interpolation function is equal to the L^2 projection on E of the divergence of the continuous function. That is, using (7),

$$\begin{aligned} \nabla_h \cdot \mathbf{v}^{\mathcal{I}}|_E &= \frac{1}{|E|} \sum_{F_i \in \partial E} \sum_{k \in \mathcal{N}_i^E} ((\mathbf{v}^{\mathcal{I}})_{ik} \cdot \mathbf{n}_i^E, 1)_{0,F_{ik}} = \frac{1}{|E|} \sum_{F_i \in \partial E} (\mathbf{v} \cdot \mathbf{n}_i^E, 1)_{F_i} \\ &= \frac{1}{|E|} (\nabla \cdot \mathbf{v}, 1)_{0,E}. \end{aligned} \tag{8}$$

In particular, by setting $\mathbf{u} = -K \nabla p$ we see that

$$\nabla_h \cdot \mathbf{u}_h^{\mathcal{I}} = \frac{1}{|E|} (\nabla \cdot (-K \nabla p), 1)_{0,E} = \frac{1}{|E|} (f, 1)_{0,E}, \tag{9}$$

a result which will be used in the convergence proof.

2.3 Reformulation of MPFA

The mimetic method defines a quadrature for each element with a quadrature matrix that is in general full, though symmetric. Only one unknown is specified for each face. The MPFA method is designed to give explicit local fluxes, a property that requires that the number of unknowns be expanded. However,

the resulting quadrature Λ matrix is sparse, with non-zero elements only if the partial fluxes share a vertex. The quadrature over the element E can therefore be decomposed into the sum of local quadratures with matrices that are of size $d \times d$, i.e, for $\mathbf{u}_h, \mathbf{v}_h \in V_h$:

$$[\mathbf{u}_h, \mathbf{v}_h]_E = \tilde{\mathbf{v}}_h^t \Lambda^E \tilde{\mathbf{u}}_h = \sum_k \tilde{\mathbf{v}}_{h,k}^t \Lambda_k \tilde{\mathbf{u}}_{h,k} \tag{10}$$

where the quadrature matrix Λ^E depends on the permeability and the mesh geometry. We set K_0^E equal to the constant permeability tensor on E such that

$$\|K - K_0^E\|_{L^\infty(E)} \lesssim h_E \qquad \forall E \in \mathcal{P}_h. \tag{11}$$

The MPFA quadrature matrix Λ_k for the O-method is then defined for each partial volume E_k as

$$\Lambda_k = R_k (K_0^E)^{-1} Q_k^{-t}. \tag{12}$$

Indicating by $i1, i2, i3$ the three partial sides that share the vertex k (in $2D$ any reference to $i3$ is simply eliminated), the two matrices R_k and Q_k are defined, as

$$R_k = \left(\bar{\mathbf{x}}_{i1}^E - \bar{\mathbf{x}}_0^E, \bar{\mathbf{x}}_{i2}^E - \bar{\mathbf{x}}_0^E, \bar{\mathbf{x}}_{i3}^E - \bar{\mathbf{x}}_0^E\right)^t \qquad \text{and} \qquad Q_k = \left(\tilde{\mathbf{n}}_{i1}^E, \tilde{\mathbf{n}}_{i2}^E, \tilde{\mathbf{n}}_{i3}^E\right). \tag{13}$$

We define the scalar product on X_h as

$$(p_h, q_h)_{X_h} = \sum_{E \in \mathcal{P}_h} (p_h, q_h)_{0,E} \qquad \forall p_h, q_h \in X_h$$

The discrete version of (2) using the MPFA quadrature is then: find $(\mathbf{u}_h, p_h) \in (V_h, X_h)$ such that

$$\begin{cases} \sum_{E \in \mathcal{P}_h} [\mathbf{u}_h, \mathbf{v}_h]_E - (p_h, \nabla_h \cdot \mathbf{v}_h)_{X_h} = 0 & \forall \mathbf{v}_h \in V_h, \\ (\nabla_h \cdot \mathbf{u}_h, q_h)_{X_h} = (f, q_h)_{0,\Omega} & \forall q_h \in X_h. \end{cases} \tag{14}$$

This formulation coincides with the MPFA formulation presented for instance in [3, 1, 20]. It is important to note that the most efficient way to solve a problem using the MPFA method is to use the standard formulation on the dual grid, which is also how one obtains the local explicit fluxes. By using the quadrature formulation (14) on the (original) grid one obtains a K^{-1} method (that is, the gradient is expressed in terms of the fluxes) with a higher number of unknowns with respect to a standard mimetic finite difference method. The quadrature formulation is however useful to analyse the convergence of the method, as we shall see.

2.4 Energy norm and assumption

We note that while the term $[\mathbf{u}_h, \mathbf{v}_h]_E$ is a scalar product when the mimetic finite difference method is used, this is in general not the case for the MPFA method,

as Λ_k can be non-symmetric. However, the matrix Λ^E can be decomposed into its symmetric and skew-symmetric parts

$$\Lambda^E = \tfrac{1}{2}(\Lambda + \Lambda^t) + \tfrac{1}{2}(\Lambda - \Lambda^t) = \Lambda_S + \Lambda_A \tag{15}$$

and similarly $\Lambda_k = (\Lambda_S)_k + (\Lambda_A)_k$. We define the following scalar product on V_h:

$$(\mathbf{u}_h, \mathbf{v}_h)_{V_h} = \sum_{E \in \mathcal{P}_h} (\mathbf{u}_h, \mathbf{v}_h)_{\Lambda_S(E)}; \qquad (\mathbf{u}_h, \mathbf{v}_h)_{\Lambda_S(E)} = \tilde{\mathbf{v}}_h^t \Lambda_S \tilde{\mathbf{u}}_h.$$

For this scalar product to be valid, Λ_s must be positive definite. We make the following assumptions on Λ_S: there exist two positive constants $\underline{c}$ and $\bar{c}$ independent of h_E and E such that $\forall \mathbf{v}_h \in V_h$ and $\forall E \in \mathcal{P}_h$

$$\underline{c}_{\Lambda(E)} h_E^{2-d} \sum_{F_i \in \partial E} \sum_{k \in \mathcal{N}_i^E} \tilde{v}_{ik}^2 \leq (\mathbf{v}_h, \mathbf{v}_h)_{\Lambda_S(E)} \leq \bar{c}_{\Lambda(E)} h_E^{2-d} \sum_{F_i \in \partial E} \sum_{k \in \mathcal{N}_i^E} \tilde{v}_{ik}^2. \tag{16}$$

The validation and implication of this assumption is discussed in the last section. We also assume that

$$c_{\Lambda(E)} = \max_k \left(\frac{\|(\Lambda_A)\|_{L^\infty(E_k)}}{\min(\lambda_k)} \right), \tag{17}$$

is finite, where λ_k denotes the eigenvalues of $(\Lambda_S)_k$.

We can now define the following norms based on the scalar products:

$$\|\mathbf{v}_h\|_{V_h}^2 = (\mathbf{v}_h, \mathbf{v}_h)_{V_h}, \qquad \|\mathbf{v}_h\|_{V_h(E)}^2 = (\mathbf{v}_h, \mathbf{v}_h)_{\Lambda_S(E)} \qquad \forall \mathbf{v}_h \in V_h \tag{18}$$

$$\|q_h\|_{X_h}^2 = (q_h, q_h)_{X_h}, \qquad \|q_h\|_{X_h(E)}^2 = (q_h, q_h)_{0,E} \qquad \forall q_h \in X_h. \tag{19}$$

3 Theoretical results

The MPFA quadrature $[\cdot,\cdot]_E$ can be seen as an approximation of the integral $(K^{-1}\cdot,\cdot)_{0,E}$, which, using the divergence theorem on the element E for $q \in H^1(\Omega)$ and $\mathbf{v} \in H(\mathrm{div}, \Omega)$ is equal to

$$\begin{aligned}(K^{-1}K\nabla q, \mathbf{v})_{0,E} &= -(q, \nabla\cdot\mathbf{v})_{0,E} + (q, \mathbf{v}\cdot\mathbf{n}^E)_{0,\partial E} \\ &= -(q, \nabla\cdot\mathbf{v})_{0,E} + \sum_{F_i \in \partial E} |F_i|^{-1} (q, \mathbf{v}\cdot\mathbf{n}_i^E |F_i|)_{0,F_i}\end{aligned}$$

where we have rewritten the border integral to more easily see the analogy with the discrete fluxes. A similar relation is thus sought for the MPFA method, indication that the MPFA quadrature is exact on linear fields.

Lemma 1. *For any linear field q the MPFA method satisfies the following discrete divergence theorem:*

$$[K_0^E \nabla q, \mathbf{v}_h]_E = -(q, \nabla_h\cdot\mathbf{v}_h)_{0,E} + \sum_{F_i \in \partial E} |F_i|^{-1} (q, \tilde{v}_i^E)_{0,F_i} \qquad \forall \mathbf{v}_h \in V_h. \tag{20}$$

Proof. Observe that the integral $(q, \nabla_h \cdot \mathbf{v}_h)_{0,E}$ is zero since the divergence is constant on the element E and the barycenter of the element is the local origin. Set $q = x_j$ with $1 \leq j \leq d$. The partial fluxes of $K_0^E \nabla q$ on the external faces of E_k are equal to $Q_k^t K_0^E \nabla q$, as $K_0^E \nabla q$ is constant and each column of the matrix Q_k corresponds to the integral of the normal vector on F_{ik}. Using the quadrature of the MPFA method (see (10) and (12)), the left-hand side of (20) is

$$\begin{aligned}[K_0^E \nabla q, \mathbf{v}_h]_E &= \sum_k \tilde{\mathbf{v}}_k^t \Lambda_k Q_k^t K_0^E \nabla x_j = \sum_k \tilde{\mathbf{v}}_k^t R_k (K_0^E)^{-1} Q_k^{-t} Q_k^t K_0^E \nabla x_j \\ &= \sum_k \tilde{\mathbf{v}}_k^t R_k \nabla x_j. \end{aligned} \tag{21}$$

Regarding the right-hand side of (20) we first note that

$$|F_i|^{-1}(q, 1)_{0,F_i} = (\bar{\mathbf{x}}_i - \bar{\mathbf{x}}_0^E)|_{x_j}.$$

We rewrite the border integral as

$$\sum_{F_i \in \partial E} |F_i|^{-1}(q, \tilde{v}_i)_{0,F_i} = \sum_{F_i \in \partial E} \Big(\sum_{k \in \mathcal{N}_i^E} \tilde{v}_{ik}^E \Big)(\bar{\mathbf{x}}_i - \bar{\mathbf{x}}_0^E)|_{x_j} = \sum_k \tilde{\mathbf{v}}_k^t R_k \nabla x_j \tag{22}$$

which proves that (22) is equal to (21) for all $\tilde{\mathbf{v}}_k$, and thus (20) is satisfied for all $\mathbf{v}_h \in V_h$. □

3.1 Well-posedness of the problem

To show the well-posedness of the problem, we will use the mesh dependent norms

$$\|\mathbf{v}_h\|_{\text{divh}}^2 = \sum_{E \in \mathcal{P}_h} \|\mathbf{v}_h\|_{\text{divh},E}^2 \qquad \|\mathbf{v}_h\|_{\text{divh},E}^2 = \|\mathbf{v}_h\|_{V_h(E)}^2 + h_E^2 \|\nabla_h \cdot \mathbf{v}_h\|_{0,E}^2 \tag{23}$$

$$\|\mathbf{v}\|_{1,h}^2 = \sum_{E \in \mathcal{P}_h} \|\mathbf{v}\|_{1,h,E}^2 \qquad \|\mathbf{v}\|_{1,h,E}^2 = \|\mathbf{v}\|_{0,E}^2 + h_E^2 |\mathbf{v}|_{1,E}^2 \tag{24}$$

in addition to the norms defined by means of the scalar products, (18) and (19).

The saddle-point problem (14) is well defined when the bilinear form $a(\mathbf{v}_h, \mathbf{w}_h) = \sum_{E \in \mathcal{P}_h} [\mathbf{v}_h, \mathbf{w}_h]_E$ is continuous and also coercive on the divergence-free subspace, while the inf-sup condition

$$\beta \|q_h\|_{X_h} \leq \sup_{\mathbf{v}_h \in V_h} \frac{(\nabla_h \cdot \mathbf{v}_h, q_h)_{X_h}}{\|\mathbf{v}_h\|_{\text{divh}}} \qquad \forall q_h \in X_h, \tag{25}$$

must be satisfied with $\beta > 0$.

The assumption (17) ensures the continuity of the bilinear form, since $\forall E \in \mathcal{P}_h$

$$[\mathbf{u}_h, \mathbf{v}_h]_E = (\mathbf{u}_h, \mathbf{v}_h)_{\Lambda_S(E)} + \tilde{\mathbf{v}}_h^t \Lambda_A \tilde{\mathbf{u}}_h \leq (1 + c_{\Lambda(E)}) \|\mathbf{u}_h\|_{V_h(E)} \|\mathbf{v}_h\|_{V_h(E)} \tag{26}$$

with $c_{\Lambda(E)}$ finite and thus

$$a(\mathbf{v}_h, \mathbf{w}_h) = \sum_{E \in \mathcal{P}_h} [\mathbf{u}_h, \mathbf{v}_h]_E \leq (1 + \max_E c_{\Lambda(E)}) \|\mathbf{u}_h\|_{V_h} \|\mathbf{v}_h\|_{V_h}.$$

The coercivity at the subspace

$$Z_h = \{\mathbf{v}_h \in V_h : (\nabla_h \cdot \mathbf{v}_h, q_h)_{X_h} = 0, \quad \forall q_h \in X_h\} \tag{27}$$

is evident since for any $\mathbf{v}_h \in Z_h$

$$\|\mathbf{v}_h\|^2_{\text{divh}} = \|\mathbf{v}_h\|^2_{V_h} = a(\mathbf{v}_h, \mathbf{v}_h). \tag{28}$$

The inf-sup condition can be proved as in [7] by first showing that for any $q_h \in X_h$ there exists $\mathbf{v}_h \in V_h$ such that $\nabla_h \cdot \mathbf{v}_h = q_h$. By solving the Laplace equation with homogeneous Dirichlet boundary conditions and q_h as the source term, that is $\Delta\psi = q_h$, and setting $\mathbf{v} \in H(\text{div}, \Omega) = \nabla\psi$, the stability of the solution ensures that

$$\|\mathbf{v}\|_{1,h} \lesssim (1 + h)\|q\|_{X_h}. \tag{29}$$

Setting $\mathbf{v}_h = \mathbf{v}^I$ using the interpolation operator defined in (6) gives the sought for solution since

$$\nabla_h \cdot \mathbf{v}_h|_E = \nabla_h \cdot \mathbf{v}^I|_E = \frac{1}{|E|}(\nabla \cdot \mathbf{v}, 1)_{0,E} = \frac{1}{|E|}(q_h, 1)_{0,E} = q_h|_E$$

Then the inf-sup condition (25) reads

$$\sup \frac{(\nabla_h \cdot \mathbf{v}_h, q_h)_{X_h}}{\|\mathbf{v}_h\|_{\text{divh}}} = \sup \frac{\|q_h\|^2_{X_h}}{\|\mathbf{v}_h\|_{\text{divh}}} \geq \beta \|q_h\|_{X_h} \quad \forall q_h \in X_h,$$

that is

$$\|q_h\|_{X_h} \geq \beta \|\mathbf{v}_h\|_{\text{divh}} \quad \forall q_h \in X_h. \tag{30}$$

In Lemma 2 we prove that

$$\|\mathbf{v}_h\|_{\text{divh}} \lesssim \|\mathbf{v}\|_{1,h}$$

which together with (29) gives

$$\|\mathbf{v}_h\|_{\text{divh}} \lesssim (1 + h)\|q\|_{X_h} \tag{31}$$

which is the necessary inf-sup condition (30).

In the following Lemma needed to prove the inf-sup condition we will make use of the trace inequality valid on sufficiently shape regular domains:

$$\|\mathbf{v}_E\|^2_{0,F_i} \leq c_F(h_E^{-1}\|\mathbf{v}_E\|^2_{0,E}) + h_E|\mathbf{v}_E|^2_{1,E} \tag{32}$$

and the following hypothesis on mesh conformity:

$$c_{f1} h_E^{d-1} \leq |F| \leq c_{f2} h_E^{d-1}. \tag{33}$$

Lemma 2. *There exists a positive constant β such that $\forall \mathbf{v} \in [H^1(E)]^d$ we have*

$$\beta \|\mathbf{v}^I\|_{divh} \leq \|\mathbf{v}\|_{1,h} \tag{34}$$

Proof. The assumption (16) applied to the interpolation of $\mathbf{v}$ states that

$$(\mathbf{v}^I, \mathbf{v}^I)_{\Lambda_S(E)} \leq \bar{c}_{\Lambda(E)} h_E^{2-d} \sum_{F_i \in \partial E} \sum_{k \in \mathcal{N}_i^E} (\tilde{v}_{ik}^I)^2. \tag{35}$$

Using the interpolation property (7), and the assumption on the mesh (33), gives

$$\begin{aligned}
\sum_{k \in \mathcal{N}_i^E} (\tilde{v}_{ik}^I)^2 &= \sum_{k \in \mathcal{N}_i^E} (\mathbf{v} \cdot \mathbf{n}_{Ei}, 1)_{0,F_{ik}}^2 \leq \sum_{k \in \mathcal{N}_i^E} \|\mathbf{v}\|_{0,F_{ik}}^2 |F_{ik}| \\
&\leq \sum_{k \in \mathcal{N}_i^E} \|\mathbf{v}\|_{0,F_{ik}}^2 \sum_{k \in \mathcal{N}_i^E} |F_{ik}| \leq (\|\mathbf{v}\|_{0,F_i}^2)^2 |F_i| \\
&\leq c_{f2} h_E^{d-1} \|\mathbf{v}\|_{0,F_i}^2
\end{aligned}$$

Inserting this result into (35) and using the interpolation result (32) we obtain

$$\begin{aligned}
(\mathbf{v}^I, \mathbf{v}^I)_{\Lambda_S(E)} &\leq \bar{c}_{\Lambda(E)} h_E \sum_{F_i \in \partial E} c_{f2} \|\mathbf{v}\|_{0,F_i}^2 \\
&\leq \bar{c}_{\Lambda(E)} h_E \sum_{F_i \in \partial E} c_{f2} c_F (h_E^{-1} \|\mathbf{v}\|_{0,E}^2 + h_E |\mathbf{v}|_{1,E}^2) \\
&\leq \bar{c}_{\Lambda(E)} \sum_{F_i \in \partial E} c_{f2} c_F (\|\mathbf{v}\|_{0,E}^2 + h_E^2 |\mathbf{v}|_{1,E}^2) \\
&\leq \tilde{\beta}_E \|\mathbf{v}\|_{1,h,E}^2
\end{aligned} \tag{36}$$

with

$$\tilde{\beta}_E = \bar{c}_{\Lambda(E)} \Big(\sum_{F_i \in \partial E} c_{f2} c_F \Big)$$

Furthermore, since

$$(\nabla_h \cdot \mathbf{v}^I, 1)_{0,E} = (\nabla \cdot \mathbf{v}, 1)_{0,E} = (\Pi_0(\nabla \cdot \mathbf{v}), 1)_{0,E}$$

we have

$$\|\nabla_h \cdot \mathbf{v}^I\|_{0,E}^2 = \|\Pi_0(\nabla \cdot \mathbf{v})\|_{0,E}^2 \leq \|\nabla \cdot \mathbf{v}\|_{0,E}^2 \leq d |\mathbf{v}|_{1,E}^2 \tag{37}$$

Combining (36) and (37) we obtain

$$\|\mathbf{v}^I\|_{\mathrm{divh},E}^2 \leq (\tilde{\beta}_E + d) \|\mathbf{v}\|_{1,h,E}^2$$

and thus (34), with

$$\beta = \Big(\sum_{E \in \mathcal{P}_h} (\tilde{\beta}_E + d) \Big)^{-\frac{1}{2}}$$

□

3.2 Convergence

Before presenting the convergence result, we look at some approximation properties and results for the Π_1 projection on E, i.e. the L_2-projection of degree 1 on E. We will make use of the poincaré type inequalities

$$\|p - \Pi_1 p\|_{0,E} \leq c_p h_E^2 \|p\|_{2,E}. \tag{38}$$
$$\|\nabla(p - \Pi_1 p)\|_{0,E} \leq c_p h_E \|p\|_{2,E}. \tag{39}$$

and apply the trace inequality (32) so that

$$\begin{aligned}\|p - \Pi_1 p\|_{0,F_i}^2 &\leq c_F(h_E^{-1}\|p - \Pi_1 p\|_{0,E}^2 + h_E|p - \Pi_1 p|_{1,E}^2) \\ &\leq c_F c_p h_E^3 \|p\|_{2,E}^2. \end{aligned}\tag{40}$$

We will also use

$$\|\nabla(\Pi_1 p)\|_{0,E}^2 \leq c_p h_E^2 \|\Pi_1 p\|_{2,E}^2 \tag{41}$$

balid on shape regular domains. From (39) and the definition of the mesh-dependent norms (23) and (24), we then obtain

$$\begin{aligned}\|\nabla(p - \Pi_1 p)\|_{1,h,E} &\leq (\|\nabla(p - \Pi_1 p)\|_{0,E}^2 + h_E^2|\nabla(p - \Pi_1 p)|_{1,E}^2)^{\frac{1}{2}} \\ &\leq (1 + c_p^2)^{\frac{1}{2}} h_E \|p\|_{2,E}. \end{aligned}\tag{42}$$

Theorem 3. *Let $(p, \mathbf{U})$ be the solution of the continuous problem (2), and let $(p_h, \mathbf{u}_h)$ be the solution of the discrete problem (14). Let $\mathbf{u}^{\mathcal{I}} \in V_h$ be the interpolant of $\mathbf{U}$ defined by (6). Then, if $p \in H^2(\Omega)$,*

$$\|\mathbf{u}^{\mathcal{I}} - \mathbf{u}_h\|_{V_h} \lesssim h\|p\|_{H^2(\Omega)}.$$

Proof. We note that $\forall \mathbf{u}_h \in V_h$,

$$\|\mathbf{u}_h\|_{V_h}^2 = \sum_{E \in \mathcal{P}_h} (\mathbf{u}_h, \mathbf{u}_h)_{\Lambda_S(E)} = \sum_{E \in \mathcal{P}_h} [\mathbf{u}_h, \mathbf{u}_h]_E.$$

Then, using the discrete problem (14),

$$\begin{aligned}\|\mathbf{u}^{\mathcal{I}} - \mathbf{u}_h\|_{V_h}^2 &= \sum_{E \in \mathcal{P}_h} [\mathbf{u}^{\mathcal{I}} - \mathbf{u}_h, \mathbf{u}^{\mathcal{I}} - \mathbf{u}_h]_E = \sum_{E \in \mathcal{P}_h} [\mathbf{u}^{\mathcal{I}}, \mathbf{u}^{\mathcal{I}} - \mathbf{u}_h]_E - \sum_{E \in \mathcal{P}_h} [\mathbf{u}_h, \mathbf{u}^{\mathcal{I}} - \mathbf{u}_h]_E \\ &= \sum_{E \in \mathcal{P}_h} [\mathbf{u}^{\mathcal{I}}, \mathbf{u}^{\mathcal{I}} - \mathbf{u}_h]_E - (p_h, \nabla_h \cdot (\mathbf{u}^{\mathcal{I}} - \mathbf{u}_h))_{X_h}\end{aligned}$$

where the second term on the right-hand side is zero due to (9) and (14). Adding and subtracting equal terms we obtain

$$\begin{aligned}\|\mathbf{u}^{\mathcal{I}}-\mathbf{u}_h\|_{V_h}^2 &= \sum_{E\in\mathcal{P}_h}[\mathbf{u}^{\mathcal{I}},\mathbf{u}^{\mathcal{I}}-\mathbf{u}_h]_E\\ &= \sum_{E\in\mathcal{P}_h}[(-K\nabla p)^{\mathcal{I}}+(K\nabla\Pi_1 p)^{\mathcal{I}},\mathbf{u}^{\mathcal{I}}-\mathbf{u}_h]_E\\ &+ \sum_{E\in\mathcal{P}_h}[(-K\nabla\Pi_1 p)^{\mathcal{I}}+(K_0^E\nabla\Pi_1 p)^{\mathcal{I}},\mathbf{u}^{\mathcal{I}}-\mathbf{u}_h]_E+\sum_{E\in\mathcal{P}_h}[(-K_0^E\nabla\Pi_1 p)^{\mathcal{I}},\mathbf{u}^{\mathcal{I}}-\mathbf{u}_h]_E\\ &= I_1+I_2+I_3 \end{aligned} \tag{43}$$

For the first term we use (26) to obtain

$$\begin{aligned}I_1 &= \sum_{E\in\mathcal{P}_h}[(-K\nabla p)^{\mathcal{I}}+(K\nabla\Pi_1 p)^{\mathcal{I}},\mathbf{u}^{\mathcal{I}}-\mathbf{u}_h]_E\\ &\leq \sum_{E\in\mathcal{P}_h}(1+c_{\Lambda(E)})\|(K\nabla(p-\Pi_1 p))^{\mathcal{I}}\|_{V_h(E)}\|\mathbf{u}^{\mathcal{I}}-\mathbf{u}_h\|_{V_h(E)}.\end{aligned}$$

From (36) we have

$$\|(K\nabla(p-\Pi_1 p))^{\mathcal{I}}\|_{V_h(E)}\leq\tilde{\beta}_E^{\frac{1}{2}}\|K\nabla(p-\Pi_1 p)\|_{1,h,E}$$

Using the approximation result (42) we then obtain

$$\|(K\nabla(p-\Pi_1 p))^{\mathcal{I}}\|_{V_h(E)}\leq\tilde{\beta}_E^{\frac{1}{2}}\|K\|_{L^\infty(E)}(1+c_p^2)^{\frac{1}{2}}h_E\|p\|_{2,E}$$

and thus

$$I_1\lesssim\sum_{E\in\mathcal{P}_h}h_E\|p\|_{2,E}\|\mathbf{u}^{\mathcal{I}}-\mathbf{u}_h\|_{V_h(E)}. \tag{44}$$

For the second term we first use (26) and the assumption on the permeability tensor (11) to obtain

$$\begin{aligned}I_2 &= \sum_{E\in\mathcal{P}_h}[((-K+K_0^E)\nabla\Pi_1 p)^{\mathcal{I}},\mathbf{u}^{\mathcal{I}}-\mathbf{u}_h]_E\\ &\leq \sum_{E\in\mathcal{P}_h}\|K-K_0^E\|_{L^\infty(E)}(1+c_{\Lambda(E)})\|(\nabla\Pi_1 p)^{\mathcal{I}}\|_{V_h(E)}\|\mathbf{u}^{\mathcal{I}}-\mathbf{u}_h\|_{V_h(E)}\\ &\lesssim \sum_{E\in\mathcal{P}_h}h_E\|(\nabla\Pi_1 p)^{\mathcal{I}}\|_{V_h(E)}\|\mathbf{u}^{\mathcal{I}}-\mathbf{u}_h\|_{V_h(E)}.\end{aligned}$$

From (36) and adding and subtracting the function p we have

$$\begin{aligned}\|(\nabla\Pi_1 p)^{\mathcal{I}}\|_{V_h(E)}\leq\tilde{\beta}_E^{\frac{1}{2}}\|\nabla\Pi_1 p\|_{1,h,E} &\leq \tilde{\beta}_E^{\frac{1}{2}}(\|\nabla p\|_{1,h,E}+\|\nabla(p-\Pi_1 p)\|_{1,h,E})\\ &\leq\tilde{\beta}_E^{\frac{1}{2}}(1+c_p h_E)\|\nabla p\|_{0,E}\end{aligned} \tag{45}$$

Applying (42), the second term of (43) is controlled by

$$I_2 \lesssim \sum_{E\in\mathcal{P}_h} h_E(1+c_p h_E)\|p\|_{2,E}\|\mathbf{u}^{\mathcal{I}}-\mathbf{u}_h\|_{V_h(E)}. \tag{46}$$

For the third term we note that $(K_0^E\nabla\Pi_1 p)^{\mathcal{I}} = (K_0^E\nabla\Pi_1 p)$ and apply the discrete divergence theorem (20) to obtain

$$\begin{aligned} I_3 &= \sum_{E\in\mathcal{P}_h}[(-K_0^E\nabla\Pi_1 p)^I, \mathbf{u}^{\mathcal{I}}-\mathbf{u}_h]_E = -\sum_{E\in\mathcal{P}_h}[K_0^E\nabla\Pi_1 p, \mathbf{u}^{\mathcal{I}}-\mathbf{u}_h]_E \\ &= -\sum_{E\in\mathcal{P}_h}\sum_{F_i\in\partial E}|F_i|^{-1}\Big(\Pi_1 p, \sum_{k\in\mathcal{N}_i^E}(\tilde{u}_{ik}^{\mathcal{I}}-\tilde{u}_{h,ik})\Big)_{0,F_i} \\ &= -\sum_{E\in\mathcal{P}_h}\sum_{F_i\in\partial E}|F_i|^{-1}(\Pi_1 p,1)_{0,F_i}\sum_{k\in\mathcal{N}_i^E}(\tilde{u}_{ik}^{\mathcal{I}}-\tilde{u}_{h,ik}) \end{aligned}$$

where $\tilde{u}_{ik}^{\mathcal{I}}$ and $\tilde{u}_{h,ik}$ indicate the partial side fluxes of respectively the interpolated exact solution and the approximated solution. Note that on a partial side shared by two elements the sum of the corresponding partial fluxes is equal to zero. Since we are applying homogeneous boundary conditions and the exact pressure solution p is continuous over an interface we obtain

$$\begin{aligned} I_3 &= \sum_{E\in\mathcal{P}_h}\sum_{F_i\in\partial E}|F_i|^{-1}(p-\Pi_1 p,1)_{0,F_i}\sum_{k\in\mathcal{N}_i^E}(\tilde{u}_{ik}^{\mathcal{I}}-\tilde{u}_{h,ik}) \\ &\leq \sum_{E\in\mathcal{P}_h}\sum_{F_i\in\partial E}|F_i|^{-\frac{1}{2}}\|p-\Pi_1 p\|_{0,F_i}\sum_{k\in\mathcal{N}_i^E}|\tilde{u}_{ik}^{\mathcal{I}}-\tilde{u}_{h,ik}| \end{aligned}$$

Noting that

$$\sum_{k\in\mathcal{N}_i^E}|\tilde{u}_{ik}^{\mathcal{I}}-\tilde{u}_{h,ik}| \leq m_i^{\frac{1}{2}}\left(\sum_{k\in\mathcal{N}_i^E}|\tilde{u}_{ik}^{\mathcal{I}}-\tilde{u}_{h,ik}|^2\right)^{\frac{1}{2}}$$

we then apply the trace inequality (40), the mesh conformity (33) and assumption (16) to obtain

$$\lesssim \sum_{E\in\mathcal{P}_h} h_E\|p\|_{2,E}\|\mathbf{u}^{\mathcal{I}}-\mathbf{u}_h\|_{V_h(E)}.$$

Summing I_1, I_2 and I_3 and simplifying we obtain Theorem 3. □

Theorem 4. *Let $(p,\mathbf{U})$ be the solution of the continuous problem (2), and let $(p_h,\mathbf{u}_h)$ be the solution of the discrete problem (14). Let $\Pi_0 p$ indicate the L^2 projection of p on each element E. Then, if $p\in H^2(\Omega)$,*

$$\|p_h-\Pi_0 p\|_{X_h} \lesssim h(\|p\|_{2,\Omega}+\|f\|_{1,\Omega})$$

Proof. The proof is based on the well-posedness of the dual problem

$$\begin{cases} -\nabla\cdot(K\nabla\psi) = \Pi_0 p - p_h & \text{in } \Omega \\ \psi = 0 & \text{on } \partial\Omega. \end{cases} \tag{47}$$

which for convex domains implies the stability result

$$\|\psi\|_{2,\Omega} \lesssim \|\Pi_0 p - p_h\|_{X_h}. \tag{48}$$

We first observe that $\nabla\cdot(K\nabla\psi)$ is a constant on each element E, so that

$$(p - \Pi_0 p, \nabla\cdot(K\nabla\psi))_{0,E} = 0. \tag{49}$$

Using the dual problem (47) in its weak form and subtracting the zero term (49), we obtain

$$\begin{aligned} \|p_h - \Pi_0 p\|_{X_h}^2 &= (p_h - \Pi_0 p, \nabla\cdot(K\nabla\psi))_{X_h} - \sum_{E\in\mathcal{P}_h} (p - \Pi_0 p, \nabla\cdot(K\nabla\psi))_{0,E} \\ &= (p_h, \nabla_h\cdot(K\nabla\psi)^{\mathcal{I}})_{X_h} - (p, \nabla\cdot(K\nabla\psi))_{0,\Omega} \end{aligned} \tag{50}$$

where we may use property (8) of the interpolation operator since p_h is constant over each element.

We now use the MPFA formulation (14) of the problem, and integrate by parts the second term on the right hand side of (50)

$$\begin{aligned} \|p_h - \Pi_0 p\|_{X_h}^2 &= \sum_{E\in\mathcal{P}_h} [\mathbf{u}_h, (K\nabla\psi)^{\mathcal{I}}]_E + (K\nabla p, \nabla\psi)_{0,\Omega} \\ &= \sum_{E\in\mathcal{P}_h} [\mathbf{u}_h, (K\nabla\psi)^{\mathcal{I}}]_E + (f, \psi)_{0,\Omega}. \end{aligned}$$

Adding and subtracting equal terms, we split the equation into four terms

$$\begin{aligned} \|p_h - \Pi_0 p\|_{X_h}^2 = &\sum_{E\in\mathcal{P}_h} [\mathbf{u}_h, (K\nabla(\psi - \Pi_1\psi))^{\mathcal{I}}]_E + \sum_{E\in\mathcal{P}_h} [\mathbf{u}_h, ((K - K_0^E)\nabla(\Pi_1\psi))^{\mathcal{I}}]_E \\ &+ \sum_{E\in\mathcal{P}_h} [\mathbf{u}_h, K_0^E\nabla(\Pi_1\psi)^{\mathcal{I}}]_E + (f, \psi)_{0,\Omega} = I_1 + I_2 + I_3 + I_4 \end{aligned} \tag{51}$$

which we examine separately, as in the proof of Theorem 3.

For the first term on the right-hand side of (51) we use (26), (36) and (42) to obtain

$$\begin{aligned} I_1 = &\sum_{E\in\mathcal{P}_h} [\mathbf{u}_h, (K\nabla(\psi - \Pi_1\psi))^{\mathcal{I}}]_E \leq \sum_{E\in\mathcal{P}_h} (1 + c_{\Lambda(E)})\|K\|_{L^\infty(E)}\|\nabla(\psi - \Pi_1\psi)^I\|_{V_h(E)}\|\mathbf{u}_h\|_{V_h(E)} \\ &\lesssim \sum_{E\in\mathcal{P}_h} h_E\|\psi\|_{2,E}\|\mathbf{u}_h\|_{V_h(E)} \end{aligned}$$

Proceeding as in the proof of Theorem 3, using (26), (11) and (45), the second term is controlled by

$$I_2 = \sum_{E\in\mathcal{P}_h} [\mathbf{u}_h, ((K - K_0^E)\nabla(\Pi_1\psi))^{\mathcal{I}}]_E \lesssim \sum_{E\in\mathcal{P}_h} h_E \|\nabla(\Pi_1\psi)^{\mathcal{I}}\|_{V_h E}\|\mathbf{u}_h\|_{V_h(E)}$$
$$\lesssim \sum_{E\in\mathcal{P}_h} h_E(1 + c_P h_E)\|\psi\|_{2,E}\|\mathbf{u}_h\|_{V_h(E)}$$

For the third term we can no longer use the discrete divergence theorem as the quadrature is not symmetric. However, we can use (26) to obtain

$$I_3 = \sum_{E\in\mathcal{P}_h} [\mathbf{u}_h, (K_0^E\nabla(\Pi_1(\psi)))^{\mathcal{I}}]_E = \sum_{E\in\mathcal{P}_h} [\mathbf{u}_h, K_0^E\nabla(\Pi_1(\psi)]_E$$
$$\leq \sum_{E\in\mathcal{P}_h} (1 + c_{\Lambda(E)})\|K_0^E\|_{L^\infty(E)}\|u_h\|_{V_h(E)}\|\nabla(\Pi_1(\psi))\|_{V_h(E)}.$$

Applying the assumption (16) and the trace inequality (32) leads to

$$\|\nabla(\Pi_1(\psi))\|^2_{V_h(E)} \leq \bar{c}_{\Lambda(E)} \sum_{F_i\in\partial E} c_{f2}c_F\|\nabla(\Pi_1(\psi))\|^2_{0,E}$$

We will now make use of (41). We also note that

$$\|\Pi_1\psi\|^2_{0,E} = (p, \Pi_1\psi)_{0,E} \leq \|\psi\|_{0,E}\|\Pi_1\psi\|_{0,E}.$$

since by definition for all q linear on E we have $(\Pi_1\psi, q)_{0,E} = (\psi, q)_{0,E}$. We may therefore conclude that

$$\|\nabla(\Pi_1(\psi))\|^2_{V_h(E)} \leq \bar{c}_{\Lambda(E)}(\sum_{F_i\in\partial E} c_{f2}c_F)c_P h^2\|\psi\|^2_{0,E}$$

and thus

$$I_3 \lesssim \sum_{E\in\mathcal{P}_h} h_E\|\psi\|_{2,E}\|u_h\|_{V_h(E)}.$$

For the last term, noting that $(1, \Pi_1\psi)_{0,E} = 0$ and using (38), we obtain

$$I_4 = (f, \psi)_{0,\Omega} = (f, \psi - \Pi_1\psi)_{0,\Omega} + (f - \Pi_0 f, \Pi_1\psi)$$
$$\leq \sum_{E\in\mathcal{P}_h} h_E^2\|f\|_{0,E}\|\psi\|_{2,E} + \sum_{E\in\mathcal{P}_h} c_p h_E\|f\|_{1,E}\|\psi\|_{2,E}.$$

From the triangle inequality, Theorem 3 and (36)

$$\|\mathbf{u}_h\|_{V_h} \leq \|\mathbf{u}^{\mathcal{I}} - \mathbf{u}_h\|_{V_h} + \|\mathbf{u}^{\mathcal{I}}\|_{V_h} \lesssim h\|p\|_{H^2(\Omega)} + \|K\nabla p\|_{1,h}$$
$$\lesssim h\|p\|_{H^2(\Omega)} + \|K\nabla p\|_{0,\Omega} + h_E|K\nabla p|_{1,\Omega} \lesssim \|p\|_{H^2(\Omega)}$$

Summing the various terms and simplifying (51) we then obtain the final result. □

4 Numerical examples

This section contains some numerical examples and a discussion of the convergence behavior with particular emphasis on the influence of the limitation given in the analysis. A fundamental part of the convergence analysis in the previous section is the assumption regarding the symmetric matrix Λ_S, namely (16), required to establish coercivity and convergence of the method. This condition is linked to the definition of the MPFA dual mesh and the permeability tensor K. To fulfill the lower bound of (16), the eigenvalues of $(\Lambda_s)_k$, cf. eq (12), for all k of E and all $E \in \mathcal{P}_h$ have to be strictly positive. To ensure this, the determinant of Λ_S must be positive, that is $\det(\Lambda_S) > \lambda_0 > 0$.

4.1 Polyhedral $2D$ mesh

In $2D$ it can easily be shown by dividing Λ^E into a symmetric and a skew-symmetric part, cf. (15), that

$$\det \Lambda^E = \det(\Lambda_S) + \det(\Lambda_A).$$

Furthermore we note that

$$\det \Lambda_k = \det R_k \det(K_0^E)^{-1} \det Q_k^{-t} = \frac{\det R_k}{\det Q_k} \det(K_0^E)^{-1}.$$

The determinant of $\det R_k$ can be visualised as the area spanned by the two vectors $\bar{\mathbf{x}}_{i1}^E - \bar{\mathbf{x}}_0^E$ and $\bar{\mathbf{x}}_{i2}^E - \bar{\mathbf{x}}_0^E$. Similarly, $\det Q_k$ is the area spanned by $\tilde{\mathbf{n}}_{i1}$ and $\tilde{\mathbf{n}}_{i2}$. We denote the respective areas A_R and A_Q. On sub-cell k we then have

$$\begin{aligned}\det((\Lambda_s)_k) = &\frac{1}{\det K_0^E}\frac{A_R}{A_Q} \\ &- \frac{1}{4A_Q^2}((\bar{\mathbf{x}}_{i1}^E - \bar{\mathbf{x}}_0^E)^t (K_0^E)^{-1}(\mathbf{x}_k^E - \bar{\mathbf{x}}_{i1}^E) - (\bar{\mathbf{x}}_{i2}^E - \bar{\mathbf{x}}_0^E)^t (K_0^E)^{-1}(\mathbf{x}_k^E - \bar{\mathbf{x}}_{i2}^E))^2\end{aligned}$$

where $\mathbf{x}_k$ indicates the coordinate of the node k, and $\mathbf{x}_k - \bar{\mathbf{x}}_{ij}$ is a vector perpendicular to $\tilde{\mathbf{n}}_{ij}$. For K-orthogonal meshes the last term vanishes, the method is symmetric and the lower bound is always fulfilled. For other quadrilateral and general polyhedral meshes the criteria in equation (16) will be the dominant mesh restrictions. For triangulations this restriction can be avoided, since there exists a symmetric MPFA with satisfactory qualities, as shown by Klausen in [17].

In our first test we look at a uniform pentagram with edge length equal to h. The pentagram is deformed by pulling two vertices uniformly out to the right, as indicated in Figure 1. The two vertices marked with a cross are fixed, while the last vertex is kept at the the axis of symmetry. For $K = I$ the criteria (16) breaks down for at least one subcell when we have pulled the vertices out by $2.6h$. Here h denotes the original edge length. This indicates that the allowed deformation is unfortunately quite small.

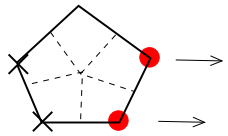

Figure 1: *The cell is fixed in vertices marked with a cross, while the vertices marked with full circles are pulled out until the criteria* (16) *is violated.*

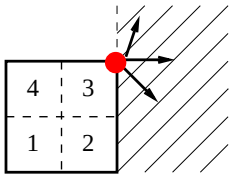

Figure 2: *The vertex marked with a full circle are pulled out in all direction of the adjacent plane.*

For our next test regarding the limitation of criteria (16) we look at a unit square with the upper right vertex placed at the origin of the plane. This vertex is then displaced in the directions contained in a half plane, as indicated in Figure 2. We set the permeability $K = I$, and number the subcells from 1 through 4 as shown. For each subcell we investigate the deformation needed for one of the eigenvalues of $(\Lambda_S)_k$ to approach zero. The result is presented in Figure 3. Each line indicates the deformation allowed in the horizontal and vertical directions before the criteria (16) breaks down. To the left of the line the criteria holds. Note that for subcell 3, the criteria (16) is satisfied for the displacements shown.

Finally we repeat the previous test, but now we use an anisotropic permeability tensor whose principal axes are aligned with the x- and the y-direction, namely $K = \mathrm{diag}(\beta, 1)$ with $\beta \in \{1, 10, 100, 500\}$. For each value of β the line in the half-plane for which the criteria (16) breaks down for at least one subcell is drawn. The result is shown in Figure 4, where the area containing the origin indicates the deformations permitted. We see that as the diffusion in the x-direction is increased (increasing β), the deformation permitted in the same direction is increased as well, while the deformation in the y-direction becomes more limited. This indicates the reason why the MPFA method is more sensitive regarding strong anisotropies compared with the mimetic finite difference method.

4.2 Hexahedral $3D$ mesh

We have tested different deformations of hexahedral $3D$ cells, starting from a uniform h-sized cube and pulling out one, two, or more vertices. We note limitations similar to the $2D$ situation, and the criteria mainly holds until we have stretched the edges by a factor between 2 and 4 with $K = I$. One specific

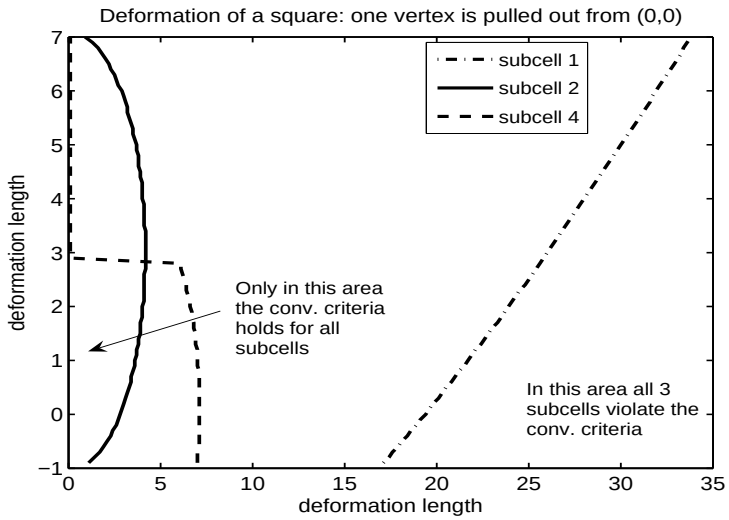

Figure 3: *Limitations of the criteria* (16) *regarding the deformation of a square when the upper right vertex, originally placed in the origin of a plane, is displaced in directions as illustrated in Figure 2.*

example is the saddle-roof box, shown in Figure 5. Starting with the uniform box of size $h\times h\times h$ we deform the upper face. Two vertices situated opposite each other on the same face are pulled upwards creating a bilinear saddle surface on top of the box. The criteria (16) breaks down for at least one of the sub-cells when the original h-sized edge are stretched to $3.45h$. Another example is the truncated pyramid, where the upper square is of size $h \times h$ while the bottom is stretch out to an $\alpha h \times \alpha h$ - square, cf. Figure 5. In this case the criteria (16) breaks down for at least one of the sub-cells when α reach 2.75.

4.3 Convergence examples

Since Λ^E depends on both the cell shape and K (see (12)), the criteria (16) is put to the test both by deforming the mesh and by varying the permeability. In Table 4.3 and 4.3 we show a numerical example in $2D$ with $K = \mathrm{diag}(\beta, 1)$ where β is increased from 1 to 1000. The mesh is shown in Figure 6, where refinement is a replication of the shown 4×4 mesh. The data is chosen so that $p(x, y) = \cos(2\pi x)\cos(2\pi y)$ is the exact solution on the domain which is the unit square. To test the behaviour of the flux calculated by the MPFA-method when Λ_S has negative eigenvalues we must modify the norm. In Table 4.3 the convergence of the flux is measured in the following norm:

$$\|\mathbf{v}_h\|^2_{V_h*} = \sum_{E\in\mathcal{P}_h} (\mathbf{v}_h, \mathbf{v}_h)_{V_h*(E)}, \quad (\mathbf{v}_h, \mathbf{v}_h)_{V_h*(E)} = \beta^{-1}(\mathbf{v}_h, \mathbf{v}_h)_{0,E} \quad \forall \mathbf{v}_h \in V_h.$$

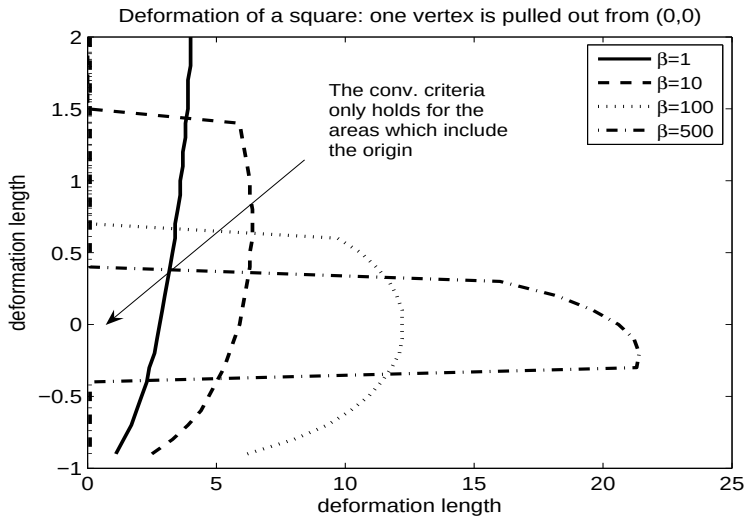

Figure 4: *Limitation of the criteria* (16) *regarding the deformation of a square when different values of* $K = diag(\beta, 1)$ *are considered.*

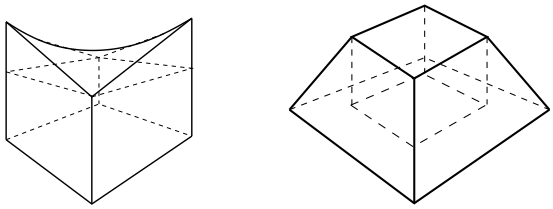

Figure 5: *The cells are stretched from a uniform box, to a saddle roof box and a truncated pyramid, until the criteria* (16) *is no longer fulfilled.*

For the error in the pressure we use the X_h-norm as previously defined. The convergence results and the percentage of sub-cells for which criteria (16) breaks down are found in Table 4.3 for the pressure and Table 4.3 for the flux. In the chosen norms the flux converges with optimal first order, while the pressure converges with second order. It seems then that the criteria (16) is not sharp in the sense that convergence can be obtained in comparable norms when the criteria is not fulfilled.

References

[1] I. Aavatsmark, T. Barkve, Ø. Bøe, and T. Mannseth "Discretization on unstructured grids for inhomogeneous, anisotropic media. I. Derivation of the methods.", SIAM J. Sci. Comput, 19 (1998), pp. 1700–1716.

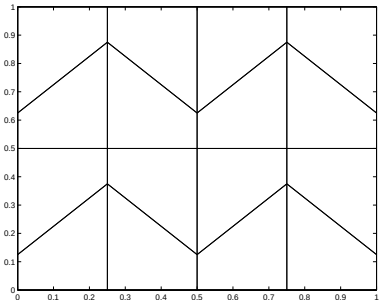

Figure 6: The 4×4 mesh, used for the numerical test shown in Table 1 and 2

β	1	10	20	50	100	1000
8×8	0.0242	0.0766	0.1082	0.1567	0.1908	0.2446
16×16	0.0059	0.0178	0.0255	0.0399	0.0549	0.1035
32×32	0.0015	0.0040	0.0055	0.0087	0.0125	0.0375
64×64	0.0004	0.0009	0.0012	0.0018	0.0025	0.0098
Conv. rate last step	1.9809	2.0955	2.1928	2.3093	2.3128	1.9299
Percentage of sub-cells violating (16)	0	25	50	75	100	100

Table 1: The error $\|p_h - p(x_{\text{cell center}})\|_{X_h}$ and the influence of violating (16)

[2] I. Aavatsmark, T. Barkve, Ø. Bøe, and T. Mannseth "Discretization on unstructured grids for inhomogeneous, anisotropic media. II. Discussion and numerical results", SIAM J. Sci. Comput, 19 (1998), pp. 1717–1736.

[3] I. Aavatsmark, "An introduction to multipoint flux approximations for quadrilateral grids", Comput. Geosci., 6 (2002), pp. 404–432.

[4] I. Aavatsmark, "Interpretation of a two-point flux stencil for skew parallelogram grids", Comput. Geosci., 11 (2007), pp. 199–206.

[5] I. Aavatsmark, T. Barkve, Ø. Bøe, and T. Mannseth "Discretization on non-orthogonal, curvilinear grids for multi-phase flow", Proc. 4th European Conference on the Mathematics of Oil Recovery, Vol. D, Røros, 1994.

β	1	10	20	50	100	1000
8×8	1.0416	1.3541	1.4895	1.6524	1.7490	1.8876
16×16	0.5025	0.6124	0.6602	0.7277	0.7797	0.9123
32×32	0.2479	0.2919	0.3067	0.3276	0.3462	0.4219
64×64	0.1234	0.1437	0.1490	0.1547	0.1595	0.1873
Conv. rate last step	1.0065	1.0229	1.0417	1.0822	1.1181	1.1714
Percentage sub-cells violating (16)	0	25	50	75	100	100

Table 2: The error $\|\mathbf{u}_h - (\mathbf{u}(x_{\text{edge center}}))^{\mathcal{I}}\|_{V_h*}$ and the influence of violating (16).

[6] I. Aavatsmark, T. Barkve, Ø. Bøe, and T. Mannseth "Discretization on non-orthogonal, quadrilateral grids for inhomogeneous, anisotropic media", J. Comput. Phys., 127 (1996), pp. 2–14.

[7] F. Brezzi, K. Lipnikov and M. Shashkov, "Convergence of mimetic finite difference method for diffusion problems on polyhedral meshes", SIAM J. Numer. Anal. 5 (2005), pp. 1872–1896.

[8] F. Brezzi, K. Lipnikov and M. Shashkov,"Convergence of mimetic finite difference method for diffusion problems on polyhedral meshes with curved faces", Math. Models Methods Appl. Sci. 2 (2006), pp. 275–297.

[9] M. G. Edwards and C. F. Rogers, "A flux continuous scheme for the full tensor pressure equation", Proc. 4th European Conference on the Mathematics of Oil Recovery, Vol. D, Røros, 1994.

[10] R. A. Klausen and G. T. Eigestad, "On the convergence of the multi-point flux approximation O-method: Numerical experiments for discontinuous permeability"., Numer. Methods Partial Diff. Eqns., 21 (2005), pp. 1079–1098.

[11] R. A. Klausen and A. F. Stephansen, "Mimetic MPFA.", Proc.11th European Conference on the Mathematics of Oil Recovery, 2008.

[12] I. Aavatsmark, G. T. Eigestad, B. T Mallison and J. M Nordbotten"A compact multipoint flux approximation method with improved robustness" Numer. Methods Partial Diff. Eqns., 24 (2008), pp. 1329–1360.

[13] K. Lipnikov, M. Shashkov and I. Yotov"Local flux mimetic finite difference methods"Numer. Math., 1 (2009), pp. 115–152.

[14] L. Agelas and R. Masson"Convergence of finite volume MPFA O type schemes for heterogeneous anisotropic diffusion problems on general meshes" C. R. Acad. Sci. Paris, 246 (2008), pp. 1007–1012.

[15] M. G. Edwards and C. F. Rogers, "Finite volume discretization with imposed flux continuity for the general tensor pressure equation", Comput. Geosci., 2 (1998), pp. 259–290.

[16] M. G. Edwards, "Unstructured, control-volume distributed, full-tensor finite-volume schemes with flow based grids", Comput. Geosci., 6 (2002), pp. 433–452.

[17] R. A. Klausen, F.A. Radu and G.T. Eigestad, "Convergence of MPFA on triangulations and for Richards' equation." International Journal for Numerical Methods in Fluids, DOI: 10.1002/fld.1787, 2008.

[18] R. A. Klausen and T. F. Russell, "Relationships among some locally conservative discretization methods which handle discontinuous coefficients", Comput. Geosci, 8 (2004), pp. 341–377.

[19] R. A. Klausen and R. Winther, "Convergence of multi point flux approximations on quadrilateral grids", Numer. Methods for PDE's, 22 (2006), pp. 1438–1454.

[20] R. A. Klausen and R. Winther, "Robust convergence of multi point flux approximation on rough grids", Numer. Math, 104 (2006), pp. 317–337.

[21] M.. Pal, M. G. Edwards, and A. R. Lamb, "Convergence study of a family of flux-continuous finite-volume schemes for the general tensor pressure equation", Int. J. Numer Meths, Fluids 51 (2006), pp. 1177-1203.

[22] M. Vohralik, "Equivalence between mixed finite element and multi-point finite volume methods", C. R. Acad. Sci. Paris., Ser. I 339 (2004).

[23] M. F. Wheeler and I. Yotov, "A multipoint flux mixed finite element method", SIAM J. Numer. Anal. 44 (2006), pp. 2082-2106.

[24] J. Hyman, M. Shashkov and S. Steinberg, "The numerical solution of diffusion problems in strongly heterogeneous non-isotropic materials", J. Comput. Phys. 132 (1997), pp. 130-148.

[25] M. Shashkov and S. Steinberg, "Solving diffusion equations with rought coefficients in rough grids", J. Comput. Phys. 129 (1996), pp. 383-405.

[26] M. Pal, M. G. Edwards and A. R. Lamb, "Convergence study of a family of flux-continuous, finite-volume schemes for the general tensor pressure equation", Internat. J. Numer. Methods Fluids 51 (2006), pp. 1177–1203